https://doi.org/10.1016/j.jpowsour.2018.02.033

Experimental and modeling study of high performance direct carbon solid oxide fuel cell with in situ catalytic steam-carbon gasification reaction

Haoran Xu[1,2], Bin Chen[1], Houcheng Zhang[1,3], Peng Tan[1], Guangming Yang[4], John T.S. Irvine[2]*, Meng Ni[1,5*]

[1] Building Energy Research Group, Department of Building and Real Estate The Hong Kong Polytechnic University, Hung Hom, Kowloon, Hong Kong, China

[2] School of Chemistry, University of St Andrews, St Andrews, Fife, KY16 9ST, UK

[3] Department of Microelectronic Science and Engineering, Ningbo University, Ningbo 315211, China

[4] Jiangsu National Synergetic Innovation Center for Advanced Materials (SICAM), College of Chemical Engineering, Nanjing Tech University, No.5 Xin Mofan Road, Nanjing 210009, P.R. China

[5] Environmental Energy Research Group, Research Institute for Sustainable Urban Development (RISUD), The Hong Kong Polytechnic University, Hung Hom, Kowloon, Hong Kong, China

Abstract:

In this paper, 2D models for direct carbon solid oxide fuel cells (DC-SOFCs) with in situ catalytic steam-carbon gasification reaction are developed. The simulation results are found to be in good agreement with experimental data. The performance of DC-SOFCs with and without catalyst are compared at different operating potential, anode inlet gas flow rate and operating temperature. It is found that adding suitable catalyst can significantly speed up the *in situ* steam-carbon gasification reaction and improve the performance of DC-SOFC with H_2O as gasification agent. The potential of syngas and electricity co-generation from the fuel cell is also evaluated, where the composition of H_2 and CO in syngas can be adjusted by controlling the anode inlet gas flow rate. In addition, the performance DC-SOFCs and the percentage of fuel in the outlet gas are both increased with increasing operating temperature. At a reduced temperature (below 800ºC), good performance of DC-SOFC can still be obtained with in-situ

catalytic carbon gasification by steam. The results of this study form a solid foundation to understand the important effect of catalyst and related operating conditions on H_2O-assisted DC-SOFCs.

Keywords: Fuel cell; carbon gasification; syngas generation

* Corresponding authors:
Email: bsmengni@polyu.edu.hk; Tel: 852-27664152; Fax: 852-27645131 (NI M).
Email: jtsi@st-andrews.ac.uk; Tel: 01334 463817 (Irvine JTS)

1. Introduction

With the increasing global attention on energy crisis and related environmental problems such as global warming and air pollution, clean utilization of energy and high efficiency energy conversion devices have received great interest from all over the world. Apart from developing renewable energy technologies, the clean and efficient utilization of fossil fuels remains to be an important topic as fossil fuels will continue to be the dominating energy source in the coming decades.

Solid oxide fuel cell (SOFC) is one of the most attractive clean and high efficient energy conversion devices for electricity power generation [1-5]. SOFCs are all solid-state devices with sandwiched structure working at high temperature (e.g. 800 °C). Its sandwiched structure includes two porous electrodes for electrochemical reactions with a dense electrolyte between them for gas separation and O^{2-} ions transportation. The electrochemical reaction between fuels (e.g. H_2) and oxidants in electrodes ensures the high energy conversion efficiency. The post-process of emission gases is also relatively easy as they are separated by the dense electrolyte. To achieve a lower operational cost and higher volumetric energy density, the direct utilization of solid carbon in SOFCs (called as direct carbon solid oxide fuel cells, DC-SOFCs) has received rising interest [6-9]. In DC-SOFCs, solid carbon is placed in the anode chamber and chemically oxidized by an agent gas (e.g. CO_2) to form gaseous fuel (e.g. CO). The produced gaseous fuel then diffuses to the anode triple phase boundary (TPB) sites for electrochemical oxidization and regenerates the agent gas. This so-called “CO shuttle mechanism” ensures the

process to take place continuously as long as there is enough solid carbon for gasification.

The gasification reaction between solid carbon and CO_2 is called reversible Boudouard reaction, which is a key reaction affecting the performance of DC-SOFC. As reported by Wu et al.[10], adopting Fe_mO_n-alkaline metal oxide catalyst greatly enhanced CO formation rate in graphite (e.g. 19 times improvement at 800 ºC) and activated carbon (e.g. 6 to 155 times improvement at 800 ºC depending on the surface area). Benefited from the largely enhanced Boudouard reaction, they successfully obtained a peak power density of 286 mW cm^{-2} at 1123 K even without external CO_2 feeding. Similarly, Tang et al. [11] significantly improved the performance of DC-SOFC (10 times higher output power density at 1073K) by loading Fe-based catalyst on the carbon fuel. Considering the importance of catalyst for Boudouard reaction in DC-SOFCs, Li et al.[12] compared Ni, K and Ca additives in carbon black and found that the catalytic effects were: K>Ni>Ca. Borja et al. [13] further studied the synergistic effect of the carbonate catalysts and Li-K carbonate system displayed the highest power densities compared with Li-Na, Li-Na-K, Li-Ba and Na-K carbonate mixtures. Apart from the use of catalysts, the carbon structure also affect the Boudouard reaction rate. Jiao et al. [14] treated coal char with alkali for structure modification to enlarge its specific surface. The output power density of DC-SOFCs was increased significantly from 62 mW cm^{-2} to 220 mW cm^{-2} at 1123K. In addition, some researchers recently proposed using H_2O instead of CO_2 as agent for carbon gasification. Ong and Ghoniem [15] developed a 1D model to compare H_2O and CO_2 as gasification agent for the indirect carbon fuel cell. The performance of the carbon

fuel cell with external carbon gasification was improved by 3-5 times with H_2O recycling from anode to the gasifier instead of CO_2 between 700 ºC and 800 ºC. In the indirect carbon SOFC, the carbon gasifier needs significant amount of heat input while the heat generated from SOFC is not well utilized. For comparison, the generated heat in the SOFC can be easily used by the carbon gasification reaction in a DC-SOFC, which could improve the overall energy efficiency of the energy efficiency of the carbon-based SOFC system. More recently, experimental and modeling works on DC-SOFC with internal carbon gasification by CO_2 and H_2O were conducted by Xu et al. [16]. Benefited from a much faster carbon gasification rate with H_2O as agent, a significant improvement of peak power density was found from 158 mW cm^{-2} (with CO_2 as agent) to 385 mW cm^{-2} (with H_2O as agent) at 1123K. Besides, using H_2O as a gasification agent offers DC-SOFC the potential for syngas and electrical power co-generation. As the syngas (CO and H_2 mixture) is an important raw material for fuel and chemical industries, sometimes both electricity and syngas are needed simultaneously. Thus, users can control the operating condition of a single device to obtain their preferred product. Although the benefits brought by using H_2O as DC-SOFC agent have been demonstrated, no study about in situ catalytic steam-carbon gasification in DC-SOFCs has been reported yet. According to Kopyscinski et al. [17], suitable catalysts like K_2CO_3 could hopefully increase the steam-carbon gasification rate. Although extra cost is needed for catalytic fuel pre-processing, adding catalyst is still a very attractive strategy for direct carbon SOFCs as not only a higher power density can be expected due to faster steam-carbon gasification rate, but also higher fuel

concentration at the anode outlet can be obtained for wider applications such as fuel and electricity co-generation. Therefore, there is a need to systematically investigate the improvement brought by in situ catalytic steam-carbon gasification in DC-SOFCs.

In order to fill the research gap mentioned-above, both experimental and numerical studies are conducted for DC-SOFCs with in situ catalytic steam-carbon gasification reaction. Experimental I-V curves and detailed numerical simulations are carried out in this paper to evaluate the catalyst effect and the potential of the DC-SOFC for electricity and fuel co-generation. The models are validated by comparing the simulation results with experimental data and good agreement is observed.

2. Model description

The chemical/electrochemical reaction, ion/electron conduction and mass/momentum transportation are fully coupled in the 2D mathematical DC-SOFC models. The schematics of DC-SOFC using H_2O as agent is shown in Fig.1. Solid carbon is placed in the anode chamber (near the porous anode) and H_2O is supplied from the anode inlet for steam-carbon gasification. The button cell has a surface area of 0.45 cm^2 with the thickness of its anode, electrolyte and cathode being 400μm, 8μm and 24μm, respectively. The cell uses Ni-YSZ (yttrium stabilized zirconium) composites as anode, bilayer YSZ/SDC (samaria-doped ceria) as electrolyte and LSCF (lanthanum strontium cobalt ferrite) as cathode. Material properties, chemical/electrochemical reaction and other tuning parameters are adopted and listed in Table 1 (ref. [18-22]) and Table 2, respectively.

2.1 Model assumption

(1) Both H_2 and CO participate in the electrochemical reactions and the TPB sites they shared is proportional to their local concentration percentage.

(2) TPB sites are distributed uniformly in the whole porous electrode. Both ionic- and electronic- conducting phases in the porous electrodes are homogeneous and continuous.

(3) Gases in the model (CO, H_2O, H_2, O_2, N_2) are ideal gases.

(4) Temperature distribution in the cell is uniform due to its small size.

(5) The volume of carbon fuel in the anode chamber does not change with time.

2.2 Chemical reactions

In anode chamber, the key chemical reaction (Eq. (1)) in the DC-SOFC is steam-carbon gasification, which converts solid carbon into gas fuels (H_2 and CO). Its reaction rate can be calculated by Eq. (2)[23]. Different tuning parameters (listed in Table 2) are used when catalyst is adopted for the reaction.

$$C + H_2O \leftrightarrow CO + H_2 \qquad (1)$$

$$R_{C\_H2O} = \frac{K_1 p_{H_2O}}{1+K_2 p_{H_2}+K_3 p_{H_2O}} \qquad (2)$$

As CO_2 is formed in the electrochemical oxidation of CO, the Boudouard reaction (Eq. (3)) is also considered. Its reaction rate can be calculated by Eq. (4)[23].

$$C + CO_2 \leftrightarrow 2CO \qquad (3)$$

$$R_{C\_CO2} = \frac{K_4 p_{CO_2}}{1+K_5 p_{CO}+K_6 p_{CO_2}} \qquad (4)$$

Due to the co-existence of H_2O and CO, water gas shift reaction (WGSR) catalyzed by nickel

in porous electrode is also considered as shown in Eq. (5). Its reaction rate can be calculated by Eqs. (6-9).[24]

$$CO + H_2O \leftrightarrow CO_2 + H_2 \qquad (5)$$

$$R_{WGSR} = k_{sf}(p_{H_2O}p_{CO} - \frac{p_{H_2}p_{CO_2}}{K_{ps}}) \qquad (6)$$

$$k_{sf} = 0.0171\exp(\frac{-103191}{RT}) \text{ (mol m}^{-3}\text{ Pa}^{-2}\text{ s}^{-1}) \qquad (7)$$

$$K_{ps} = \exp(-0.2935Z^3 + 0.6351Z^2 + 4.1788Z + 0.3169) \qquad (8)$$

$$Z = \frac{1000}{T} - 1 \qquad (9)$$

2.3 Electrochemical reaction

Both H_2 and CO produced in the chamber will transport to anode TPB sites where they electrochemically react with O^{2-} and release electrons as shown in Eq. (10) and Eq. (11). The O^{2-} ions transport through the electrolyte from the cathode, where the O_2 molecules are reduced as shown in Eq. (12).

$$H_2 + O^{2-} \rightarrow H_2O + 2e^- \qquad (10)$$

$$CO + O^{2-} \rightarrow CO_2 + 2e^- \qquad (11)$$

$$O_2 + 4e^- \rightarrow 2O^{2-} \qquad (12)$$

Based on the above equations, respective equilibrium potentials (E_{eq}) for H_2 and CO as fuel can be calculated as Eq. (13) and Eq. (14)

$$E_{CO} = E^0_{CO} + \frac{RT}{2F}\ln\left[\frac{P^L_{CO}(P^L_{O_2})^{1/2}}{P^L_{CO_2}}\right] \qquad (13)$$

$$E_{H_2} = E^0_{H_2} + \frac{RT}{2F}\ln\left[\frac{P^L_{H_2}(P^L_{O_2})^{1/2}}{P^L_{H_2O}}\right] \qquad (14)$$

Here E^0 is the standard potential (V), R is the universal gas constant (8.3145 J mol^{-1} K^{-1}), T is

the operating temperature (K), F is the Faraday constant (96485 C mol^{-1}). P^L is the local gas partial pressure (Pa). The values of E_{CO}^0 and $E_{H_2}^0$ can be calculated by Eq. (15) and Eq. (16):

$$E_{CO}^0 = 1.46713 - 0.0004527T \text{ (V)} \qquad (15)$$

$$E_{H_2}^0 = 1.253 - 0.00024516T \text{ (V)} \qquad (16)$$

It should be noted that the equilibrium potentials calculated by Eq. (13) and Eq. (14) are equal at an open circuit condition. When current is extracted from DC-SOFC, the equilibrium potentials for H_2 fuel and CO fuel become different due to the different overpotential losses involved in electrochemical oxidation of H_2 and CO.

The operating potential (V) can be calculated by equilibrium potential and operating overpotential losses (V) as shown in Eq. (17):

$$V = E_{eq} - \eta_{act} - \eta_{ohmic} \qquad (17)$$

The operating overpotential loss includes activation overpotential loss (η_{act}) and ohmic loss (η_{ohmic}). η_{act} reflects the potential barrier for the electrochemical reaction to overcome, which can be described by Butler-Volmer equation as shown in Eq. (17).

$$i = i_0 \left\{ \exp\left(\frac{\alpha n F \eta_{act}}{RT}\right) - \exp\left(\frac{(1-\alpha) n F \eta_{act}}{RT}\right) \right\} \qquad (17)$$

where i is the operating current density (A m^{-2}), i_0 is the exchange current density (A m^{-2}), α is the electron transfer coefficient and n is the number of transferred electrons per electrochemical reaction. Considering temperature effect, i_0 can be further expressed as Eq. (18).

$$i_0 = \gamma \exp\left(-\frac{E_{act}}{RT}\right) \qquad (18)$$

where γ (A m^{-2}) is the pre-exponential factor and E_{act} is the activation energy level (J mol^{-1}). The ohmic overpotential (η_{ohmic}) is related to the current intensity and ionic/electronic conductivity of the cell, and can be calculated by Ohm law. More detailed information can be found in our previous works [25-28].

2.4 Mass and momentum transport

Extended Fick's model is used to calculate the rate of mass transport ($N_i, mol\ m^{-3}\ s^{-1}$) in channels and porous electrodes as shown in Eq. (19)[29]:

$$N_i = -\frac{1}{RT}\left(\frac{B_0 y_i P}{\mu}\frac{\partial \mathrm{P}}{\partial \mathrm{z}} - D_i^{eff}\frac{\partial (y_i \mathrm{P})}{\partial \mathrm{z}}\right)\ (i = 1, \dots, n) \qquad (19)$$

where B_0 is the permeability (m^2) of the porous electrodes, y_i is the mole fraction of component i, μ is the gas viscosity (N m^{-1} s^{-1}) and D_i^{eff} is the overall effective diffusion coefficient (m^2 s^{-1}) of component i in the porous electrodes, which can be calculated by Eq. (20) [30]:

$$D_i^{eff} = \frac{\varepsilon}{\tau}\left(\frac{1}{D_{im}^{eff}} + \frac{1}{D_{ik}^{eff}}\right)^{-1} \qquad (20)$$

where ε is the porosity, τ is the tortuosity factor, D_{ik}^{eff} and D_{im}^{eff} are Knudsen diffusion coefficient (m^2 s^{-1}) and molecular diffusion coefficient (m^2 s^{-1}), respectively. Detailed calculation of D_{im}^{eff} and D_{ik}^{eff} can be found in ref. [31]. It should also be noted that the Knudsen diffusion mechanism is neglected in the gas channels as the channel size is considerably larger than the mean-free path of the molecular species.

Navier-Stokes (N-S) equation including the Darcy's term is used to describe the momentum transport of gas species in porous electrodes as shown in Eq. (21):

$$\rho \frac{\partial u}{\partial t} + \rho u \nabla u = -\nabla p + \nabla[\mu \left(\nabla u + (\nabla u)^T\right) - \frac{2}{3}\mu \nabla u\Big] - \frac{\varepsilon \mu u}{k} \qquad (21)$$

where ρ (kg m^{-3}) is the gas density and u (m s^{-1}) is the velocity vector. When the last term on the right side is neglected, Eq. (20) is reduced to conventional N-S equation for momentum conservation in gas channels.

2.5 Model solution

Electric potentials are specified at the two electrodes while two ends of the cell are electrically insulated. Inflow gas mole fraction and flow rate (SCCM) are given at the inlets. The outflow condition is specified at the outlets of the gas channels. Zero flux is specified at the end of the electrodes and pressure condition is specified at the outlets of the two gas channels.

The model is solved at given operating conditions such as electric potentials, temperature, inlet gas flow rate and mole fraction. The output of the model includes distributions of the electrochemical reaction rates, chemical reaction rates and mole fraction of gas species in the cell. The commercial software COMSOL MULTIPHYSICS® is employed for the numerical simulation.

3 Results and discussion

3.1 Experiments for model validation

The fuel cell adopted in this study for model validation employed Ni-YSZ as anode supporting the bilayer YSZ/SDC electrolyte and LSCF cathode. Na_2CO_3 was adopted as the catalyst to enhance the steam-carbon gasification reaction. For a typical synthesis, 0.015 mole catalyst was dissolved into 30 ml de-ionized water. Then 1 mole activated carbon was added to the

solution under vigorous stirring for 12 hours. The colloid was dried at 110 ºC for 4 hours and then calcined at 500 ºC in nitrogen for 2 hours. It should be noted that the present study is the first attempt to improve the performance of DC-SOFC by in-situ catalytic steam-gasification of carbon. The focus is to demonstrate the effect of catalyst on power generation and syngas co-generation. The lab-scale impregnation method for catalyst addition to carbon fuel ensures good contact between the carbon particles and the catalyst, which could facilitate carbon gasification and is beneficial to DC-SOFC. However, the impregnation method may not be practical for large-scale applications due to the relatively high cost. For practical applications, industrial scale carbon/coal gasification technology should be adopted. For example, physical mixing in a fluidized bed offers a simple and low cost option and can be employed for large-scale applications.

For the fuel cell test, the bottom cell was sealed onto a quartz tube by silver paste. The anode and cathode surfaces were printed with silver layers for current collection. 0.2 g solid carbon was fixed by asbestos in the anode chamber. A quartz tube was positioned beneath the carbon layer for introducing steam. The inlet gas flow rate of anode was set as 90 SCCM (standard conditions). 30 SCCM H_2O was carried into anode by 60SCCM N_2 in the test. The operating temperature was kept constant at 850 $^\circ$C during the test. Current-voltage values were collected based on the four-terminal configuration. The schematic designs for fuel cell tests could be found in ref. [10].

The modeling results of current-voltage characteristics for DC-SOFCs using H_2O as agent are

compared with experimental data as shown in Fig. 2. The quite small difference between the modeling results and experimental data validates the present model. The same structure and tuning parameters are used in the subsequent parametric simulations. It should be mentioned that the activated carbon is use in the experiments for model validation. When other types of carbon are used, the carbon gasification reaction kinetics could be different due to the different properties of carbon fuels. However, the proposed model can be easily applied to DC-SOFC with different types of carbon fuels by modifying the carbon oxidation reaction kinetics.

3.2 Effect of applied voltage

The voltage-current density-power density curves of DC-SOFCs using H_2O as agent are shown in Fig. 3. The detailed operating conditions are listed in Table 3.

As can be seen in Fig. 3, the cell with in situ catalytic steam-carbon gasification has a much better performance compared with the cell without catalyst. By adding catalyst, the peak power density of the cell increases from about 3000 W m^{-2} to 4600 W m^{-2}, with the maximum current density increasing from about 10000 A m^{-2} to 23000 A m^{-2}. This significant performance improvement is mainly caused by the faster steam-carbon gasification kinetics. As can be seen in Fig. 4(a) and Fig. 4(b), the peak steam-carbon gasification reaction rate increases from 11.1 mol m^{-3} s^{-1} to 292 mol m^{-3} s^{-1} with most parts in catalytic carbon layer being larger than 50 mol m^{-3} s^{-1}. Consequently, the mole fraction of the fuel (both H_2 and CO) in anode is significantly improved from about 0.1 to about 0.4 as shown in Fig. 4(c) and Fig. 4(d). The high fuel concentration indicates the potential for syngas and electricity co-generation in DC-SOFC with

in situ catalytic gasification.

It should also be noted that the fuel concentration distribution in anode is significantly affected by both steam-carbon gasification reaction and applied voltage. As can be found in Fig.5(a), the H_2 mole fraction obtains a sharp increase to 0.4 in carbon layer at 0.9 V applied voltage, while it decreases quickly to 0.2 in the area close to anode at 0.1 V applied voltage. The relationship between electrochemical performance and syngas molar fraction on the anode surface is further shown in Fig. 5(b). The syngas molar fraction exceeds 80% at small operating current density but decreases to be less than 50% at a current density of 23000 A m^{-2}. Thus, a high operating potential is more favored to maintain a high fuel concentration in the anode outlet gas.

3.3 Effect of anode inlet gas flow rate

In DC-SOFCs using H_2O as agent, steam is introduced to the anode inlet as it participates in the carbon gasification reaction, however, the inlet steam can dilute fuel concentration on the other hand. Thus, it should be careful to choose a suitable steam flow rate in operation. For the study of anode inlet gas flow rate effect, the operating parameters are listed in Table 4.

As can be seen in Fig. 6, the performance of the fuel cell increases first at small anode gas flow rate, while decreases quickly at large flow rate. A small steam flow rate is more suitable for the fuel cell as it reaches the peak current density at 10 SCCM in this case. However, no significant decrease of current density is observed in a wide flow rate range when catalyst is added in the

fuel cell. Besides, a large steam flow rate is more favored under the fast in situ catalytic gasification reaction with its peak current density being obtained at 40 SCCM flow rate.

In addition, the mole fraction of H_2 and CO in anode is also significantly affected by inlet steam flow rate as can be seen in Fig. 7(a). Apart from different electrochemical reaction kinetics, the reaction rate of WGSR is another key factor to the mole fraction change of H_2 and CO (as shown in Fig. 7(b)) since steam-carbon gasification produces equal amount of H_2 and CO. At small gas flow rates, more H_2 than CO is consumed by electrochemical reaction due to the faster reaction kinetics of H_2, in the meanwhile, the lack of steam favors WGSR to convert H_2 and CO_2 into H_2O and CO in anode (shown as negative value of WGSR in Fig. 7(b)). As a result, more CO than H_2 is left in anode. With an increase of steam flow rate, the WGSR rate turns to positive and keeps growing, while the Boudouard reaction rate remains at a small value. Consequently, the mole fraction of CO keeps decreasing, while the mole fraction of H_2 keeps rising to exceed CO and remains at a relative high level. This phenomenon indicates that the outlet gas composition from anode can be adjusted by controlling the inlet gas flow rate.

3.5 Effect of operating temperature

The operating temperature affects not only the electrochemical kinetics but also the chemical reaction rate, thus, both the output power and the fuel percentage (H_2 & CO) in outlet gas will be significantly changed at different operating temperature. For the study of temperature effect, the operating parameters are listed in Table 5.

As can be seen in Fig. 8(a), the current density of DC-SOFC with H_2O as agent is increased at a higher temperature. The existence of catalyst improves the performance of DC-SOFC especially at a low operating temperature, where a large improvement can be found (4 times improvement at 923 K and 1.4 times improvement at 1173 K). Although the output electricity power improvement by adding catalyst is not that significant at high operating temperature, the fuel percentage in outlet gas is largely improved as shown in Fig. 8(b). Benefited from faster chemical reaction kinetics as a higher temperature, the fuel percentage in outlet gas increases from 0.15% at 923 K to 20% at 1173 K without catalyst, while a percentage of 85% of fuel in the outlet gas can be obtained with the help of catalyst at 1173 K. The high fuel concentration indicates an excellent potential for fuel (H_2 & CO) and electricity cogeneration in DC-SOFC with in situ catalytic steam-carbon gasification.

4 Conclusion

Both experimental testing and mathematical modeling are conducted to study the performance of DC-SOFCs with in situ catalytic gasification of carbon by H_2O. The model is compared and validated by experimental results. Parametric analyses are carried out to investigate the effects of operating potential, anode inlet gas flowrate and operating temperature on the performance of the cell. The performance of DC-SOFCs with and without catalyst are also compared to evaluate the improvement by adding catalyst for steam-carbon gasification in DC-SOFCs.

In situ catalytic steam-carbon gasification largely increases the gas fuel production rate for

electrochemical reaction, which brings a significant improvement of output power density. A peak power density of about 4600 W m^{-2} is obtained with the help of catalyst compared with that of 3000 W m^{-2} without catalyst. The high fuel percentage in anode outlet gas is also obtained due to the faster gasification reaction with catalyst. It is found that the mole fraction of H_2 and CO in the outlet gas is significantly affected by the inlet gas flow rate. The mole fraction of CO is larger than H_2 at small inlet gas flow rate (< 100 SCCM), while H_2 exceeds CO at high inlet gas flow rate (> 100 SCCM). Thus, it could be possible to adjust the fuel component by controlling the inlet gas flow rate. The operating temperature also significantly affect the fuel percentage in outlet gas, where a high fuel percentage (84% at 1173 K) can be obtained, indicating the possibility for fuel and electricity co-generation in DC-SOFC with H_2O as agent by integrating in situ catalytic steam-carbon gasification.

Acknowledgement

This research is supported by a grant (PolyU 152127/14E) from Research Grant Council, University Grants Committee, Hong Kong SAR, a grant from Environment and Conservation Fund (ECF 54/2015), Hong Kong SAR, and a grant from Research Institute for Sustainable Urban Development (RISUD) (1-ZVEA).

We gratefully acknowledge the financial support of the National Science Foundation of China (Grant No. 51406091).

Nomenclature

Abbreviation

DC-SOFC	Direct-carbon solid oxide fuel cell
LSCF	Lanthanum strontium cobalt ferrite
SCCM	Standard cubic centime per minute

SDC	Samaria-doped ceria
SOFC	Solid oxide fuel cell
TPB	Triple phase boundary
WGSR	Water gas shift reaction
YSZ	Yttrium stabilized zirconium

Roman

B_0	Permeability coefficient, m^2
c_{CO_2}	Mole concentration of carbon dioxide, $mol \cdot m^{-3}$
c_{H_2O}	Mole concentration of water, $mol \cdot m^{-3}$
D_i^{eff}	Effective diffusivity of species i, $m^2 \cdot s^{-1}$
D_{ik}^{eff}	Knudsen diffusion coefficient of i, $m^2 \cdot s^{-1}$
D_{im}^{eff}	Molecular diffusion coefficient of i, $m^2 \cdot s^{-1}$
E_{act}	Activation energy, $J \cdot mol^{-1}$
E_{CO}	Equilibrium potential for carbon monoxide oxidization, V
E_{CO}^0	Standard equilibrium potential for carbon monoxide oxidization, V
E_{eq}	Equilibrium Nernst potential, V
E_{H_2}	Equilibrium potential for hydrogen oxidization, V
$E_{H_2}^0$	Standard equilibrium potential for hydrogen oxidization, V
F	Faraday constant, 96485 $C \cdot mol^{-1}$
i_o	Exchange current density, $A \cdot m^{-2}$
n	Number of electrons transferred per electrochemical reaction
N_i	Flux of mass transport, $kg \cdot m^{-3} \cdot s^{-1}$
p	(partial) Pressure, Pa
R	Gas constant, 8.314 $J \cdot mol^{-1} \cdot K^{-1}$
R_{C_CO2}	Reaction rate of Boudouard reaction, $mol \cdot m^{-3} \cdot s^{-1}$
R_{C_H2O}	Reaction rate of steam-carbon gasification, $mol \cdot m^{-3} \cdot s^{-1}$
R_{WGSR}	Reaction rate of water gas shift reaction, $mol \cdot m^{-3} \cdot s^{-1}$
T	Temperature, K
u	Velocity field, $m^3 \cdot s^{-1}$
V	Volume fraction
y_i	Mole fraction of component i

Greek letters

α	Charge transfer coefficient
β_{H_2}	Electrochemical kinetics parameter for H_2
ε	Porosity
η_{act}	Activation polarization, V
η_{ohmic}	Ohmic polarization, V
κ	Permeability, m^2
μ	Dynamic viscosity of fluid, Pa·s
ρ	Fluid density, $kg \cdot m^{-3}$
σ	Conductivity, S/m
γ	Pre-exponential factor, $A\ m^{-2}$
τ	Tortuosity
∅	Potential, V

Subscripts

an	Anode
ca	Cathode

co	Carbon monoxide
H_2	Hydrogen
l	Ionic phase
s	Electronic phase

Superscripts

0	Parameter at equilibrium conditions
eff	Effective
L	Local

Reference

[1] Park S, Vohs JM, Gorte RJ. Direct oxidation of hydrocarbons in a solid-oxide fuel cell. Nature. 2000;404:265-7.
[2] Shao ZP, Haile SM. A high performance cathode for the next generation of solid oxide fuel cells, Nature. 2004; 431: 170-173.
[3] Ruiz-Morales JC, Canales Vazquez J, Savaniu CD, Marrero-Lopez D, Zhou W, Irvine JTS, Disruption of extended defects in solid oxide fuel cell anodes for methane oxidation. Nature. 2006; 439: 568-571.
[4] Wachsman ED, Lee KT, Lowering the temperature of solid oxide fuel cells. Science. 2011; 334(6058): 935-939.
[5] Ni M, Modeling of solid oxide fuel cells. Science Bulletin. 2016. 61(17): 1311-1312.
[6] Cai WZ, Liu J, Yu FY, Zhou Q, Zhang YP, Wang XQ, Liu ML, Ni M. A high performance direct carbon solid oxide fuel cell fueled by Ca-loaded activated carbon. International Journal of Hydrogen Energy. 2017;42(33):21167-21176.
[7] Giddey S, Badwal SPS, Kulkarni A, Munnings C. A comprehensive review of direct carbon fuel cell technology. Progress in Energy and Combustion Science. 2012;38:360-99.

[8] Gür TM. Critical Review of Carbon Conversion in “Carbon Fuel Cells”. Chemical Reviews. 2013;113:6179-206.
[9] Jiang CR, Ma JJ, Corre G, Jain SL, Irvine JTS. Challenges in developing direct carbon fuel cells. Chemical Society Reviews. 2017; 46: 2889-2912.
[10] Wu Y, Su C, Zhang C, Ran R, Shao Z. A new carbon fuel cell with high power output by integrating with in situ catalytic reverse Boudouard reaction. Electrochemistry Communications. 2009;11:1265-8.
[11] Tang Y, Liu J. Effect of anode and Boudouard reaction catalysts on the performance of direct carbon solid oxide fuel cells. International Journal of Hydrogen Energy. 2010;35:11188-93.
[12] Li C, Shi Y, Cai N. Performance improvement of direct carbon fuel cell by introducing catalytic gasification process. Journal of Power Sources. 2010;195:4660-6.
[13] Cantero-Tubilla B, Xu C, Zondlo JW, Sabolsky K, Sabolsky EM. Investigation of anode configurations and fuel mixtures on the performance of direct carbon fuel cells (DCFCs). Journal of Power Sources. 2013;238:227-35.
[14] Jiao Y, Zhao J, An W, Zhang L, Sha Y, Yang G, et al. Structurally modified coal char as a fuel for solid oxide-based carbon fuel cells with improved performance. Journal of Power Sources. 2015;288:106-14.
[15] Ong KM, Ghoniem AF. Modeling of indirect carbon fuel cell systems with steam and dry gasification. Journal of Power Sources. 2016;313:51-64.
[16] Xu H, Chen B, Zhang H, Sun Q, Yang G, Ni M. Modeling of direct carbon solid oxide fuel cells with H2O and CO2 as gasification agents. International Journal of Hydrogen Energy. 2017;42:15641-51.
[17] Kopyscinski J, Lam J, Mims CA, Hill JM. K2CO3 catalyzed steam gasification of ash-free coal. Studying the effect of temperature on carbon conversion and gas production rate using a drop-down reactor. Fuel. 2014;128:210-9.
[18] Shi Y, Cai N, Li C, Bao C, Croiset E, Qian J, et al. Modeling of an anode-supported Ni–YSZ|Ni–ScSZ|ScSZ|LSM–ScSZ multiple layers SOFC cell: Part I. Experiments, model development and validation. Journal of Power Sources. 2007;172:235-45.
[19] Luo Y, Shi YX, Li WY, Ni M, Cai NS, Elementary reaction modeling and experimental characterization of solid oxide fuel-assisted steam electrolysis cells. International Journal of Hydrogen Energy. 2014. 39(20): 10359-10373.
[20] Eguchi K. Ceramic materials containing rare earth oxides for solid oxide fuel cell. J Alloy Compd. 1997;250:486-91.
[21] Fan B, Yan J, Yan X. The ionic conductivity, thermal expansion behavior, and chemical compatibility of La0.54Sr0.44Co0.2Fe0.8O3-δ as SOFC cathode material. Solid State Sciences. 2011;13:1835-9.
[22] Tai LW, Nasrallah MM, Anderson HU, Sparlin DM, Sehlin SR. Structure and electrical properties of La1 − xSrxCo1 − yFeyO3. Part 2. The system La1 − xSrxCo0.2Fe0.8O3. Solid State Ionics. 1995;76:273-83.
[23] Huang Z, Zhang J, Zhao Y, Zhang H, Yue G, Suda T, et al. Kinetic studies of char gasification by steam and CO2 in the presence of H2 and CO. Fuel Processing Technology. 2010;91:843-7.
[24] Ni M. Modeling of SOFC running on partially pre-reformed gas mixture. International Journal of Hydrogen Energy. 2012;37:1731-45.
[25] Xu H, Chen B, Liu J, Ni M. Modeling of direct carbon solid oxide fuel cell for CO and electricity cogeneration. Applied Energy. 2016;178:353-62.
[26] Xu H, Chen B, Ni M. Modeling of Direct Carbon-Assisted Solid Oxide Electrolysis Cell

(SOEC) for Syngas Production at Two Different Electrodes. Journal of The Electrochemical Society. 2016;163:F3029-F35.
[27] Xu H, Chen B, Irvine J, Ni M. Modeling of CH4-assisted SOEC for H2O/CO2 co-electrolysis. International Journal of Hydrogen Energy. 2016;41:21839-49.
[28] Chen B, Xu HR, NI M, Modelling of finger-like channelled anode support for SOFCs application, Science Bulletin. 2016; 61(17): 1324-1332.
[29] Suwanwarangkul R, Croiset E, Fowler MW, Douglas PL, Entchev E, Douglas MA. Performance comparison of Fick's, dusty-gas and Stefan–Maxwell models to predict the concentration overpotential of a SOFC anode. Journal of Power Sources. 2003;122:9-18.
[30] Ni M, An electrochemical model for syngas production by co-electrolysis of H_2O and CO_2. Journal of Power Sources. 2012; 202: 209-216.
[31] Todd B, Young JB. Thermodynamic and transport properties of gases for use in solid oxide fuel cell modelling. Journal of Power Sources. 2002;110:186-200.

List of Tables

Table 1 Material properties [18-22]

Parameters	**Value or expression**	**Unit**
Ionic conductivity		
YSZ	$3.34 \times 10^4 e^{\frac{-10300}{T}}$	Sm^{-1}
SDC	$\frac{100}{T} \times 10^{5.48077-\frac{3792.53}{T}}$	Sm^{-1}
LSCF	$\frac{100}{T} \times 10^{2.51289-\frac{3036.75}{T}}$	Sm^{-1}
Electronic conductivity		
LSCF	$\frac{100}{T} \times 10^{4.32576+\frac{1204.26}{T}}$	Sm^{-1}
Ni	$3.27 \times 10^6 - 1065.3T$	Sm^{-1}
Porosity		
Cathode	0.2	
Anode	0.6	
Anode volume fraction		
YSZ	0.4	
Ni	0.6	
S_{TPB}		
Cathode layer	2.14×10^5	m^2m^{-3}
Anode layer	2.14×10^5	m^2m^{-3}
Electrode tortuosity	3	
Solid carbon	Activated carbon (Aladdin, Shanghai, China; A. R.)	

Table 2 Reaction parameters

Parameter	**Value**	**Unit**
Chemical reaction without catalyst		
K_1	1.03×10^{-3}	s mol kg^{-1} m^{-2}
K_2	9.88×10^{-4}	Pa^{-1}
K_3	8.13×10^{-5}	Pa^{-1}
K_4	3.11×10^{-5}	s mol kg^{-1} m^{-2}
K_5	1.25×10^{-3}	Pa^{-1}
K_6	3.82×10^{-5}	Pa^{-1}
Chemical reaction with catalyst		
K_1	3.87×10^{-2}	s mol kg^{-1} m^{-2}
K_2	9.88×10^{-4}	Pa^{-1}
K_3	8.13×10^{-5}	Pa^{-1}
K_4	1.17×10^{-3}	s mol kg^{-1} m^{-2}
K_5	1.25×10^{-3}	Pa^{-1}
K_6	3.82×10^{-5}	Pa^{-1}
Electrochemical reaction		
γ_{H_2}	3.68×10^{9}	A m^{-2}
E_{act,H_2}	1.2×10^{5}	J mol^{-1}
γ_{O_2}	3.48×10^{9}	A m^{-2}

E_{act,O_2}	1.2×10^5	J mol^{-1}
γ_{CO}	1.67×10^9	A m^{-2}
$E_{act,CO}$	1.2×10^5	J mol^{-1}
α_{H_2}	0.5	
α_{CO}	0.5	
α_{O_2}	0.85	

Table 3 Operation parameters for operating potential effect study in DC-SOFCs

Parameter	**Value**	**Unit**
Operating potential	0 – 1	V
Anode inlet gas flow rate	90	SCCM
Cathode inlet gas flow rate	10	SCCM
Anode gas composition	H_2O	
Cathode gas composition	Air	
Temperature	1123	K

Table 4 Operation parameters for anode inlet gas flow rate effect study in DC-SOFCs

Parameter	**Value**	**Unit**
Operating potential	0.5	V
Anode inlet gas flow rate	1 -200	SCCM
Cathode inlet gas flow rate	10	SCCM
Anode gas composition	H_2O	
Cathode gas composition	Air	
Temperature	1123	K

Table 5 Operation parameters for temperature effect study in DC-SOFCs

Parameter	**Value**	**Unit**
Operating potential	0.5	V
Anode inlet gas flow rate	90	SCCM
Cathode inlet gas flow rate	10	SCCM
Anode gas composition	H_2O	
Cathode gas composition	Air	
Temperature	923 - 1173	K

List of Figures

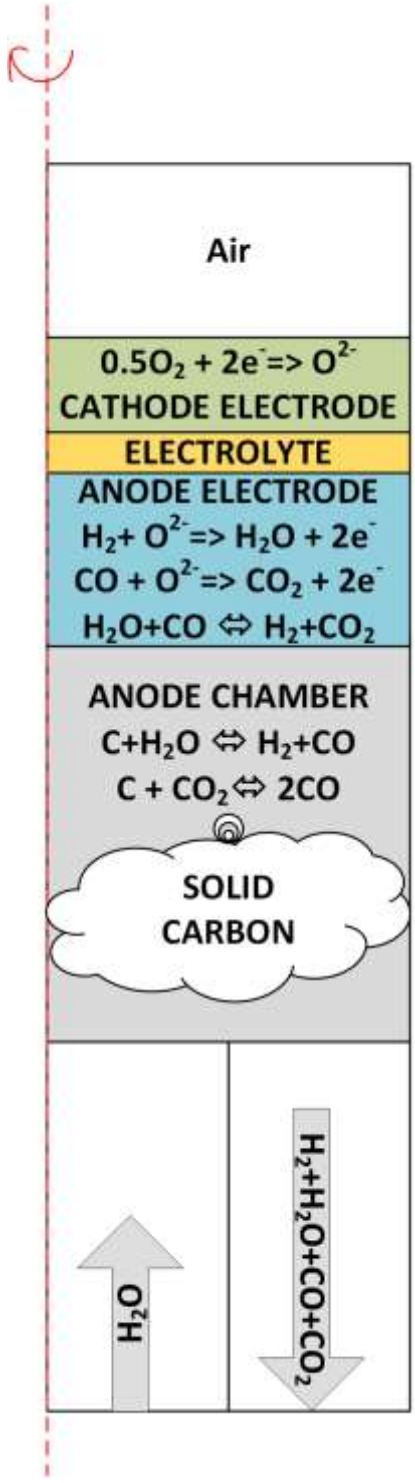

Fig.1. Schematic of DC-SOFC using H_2O as gasification agent.

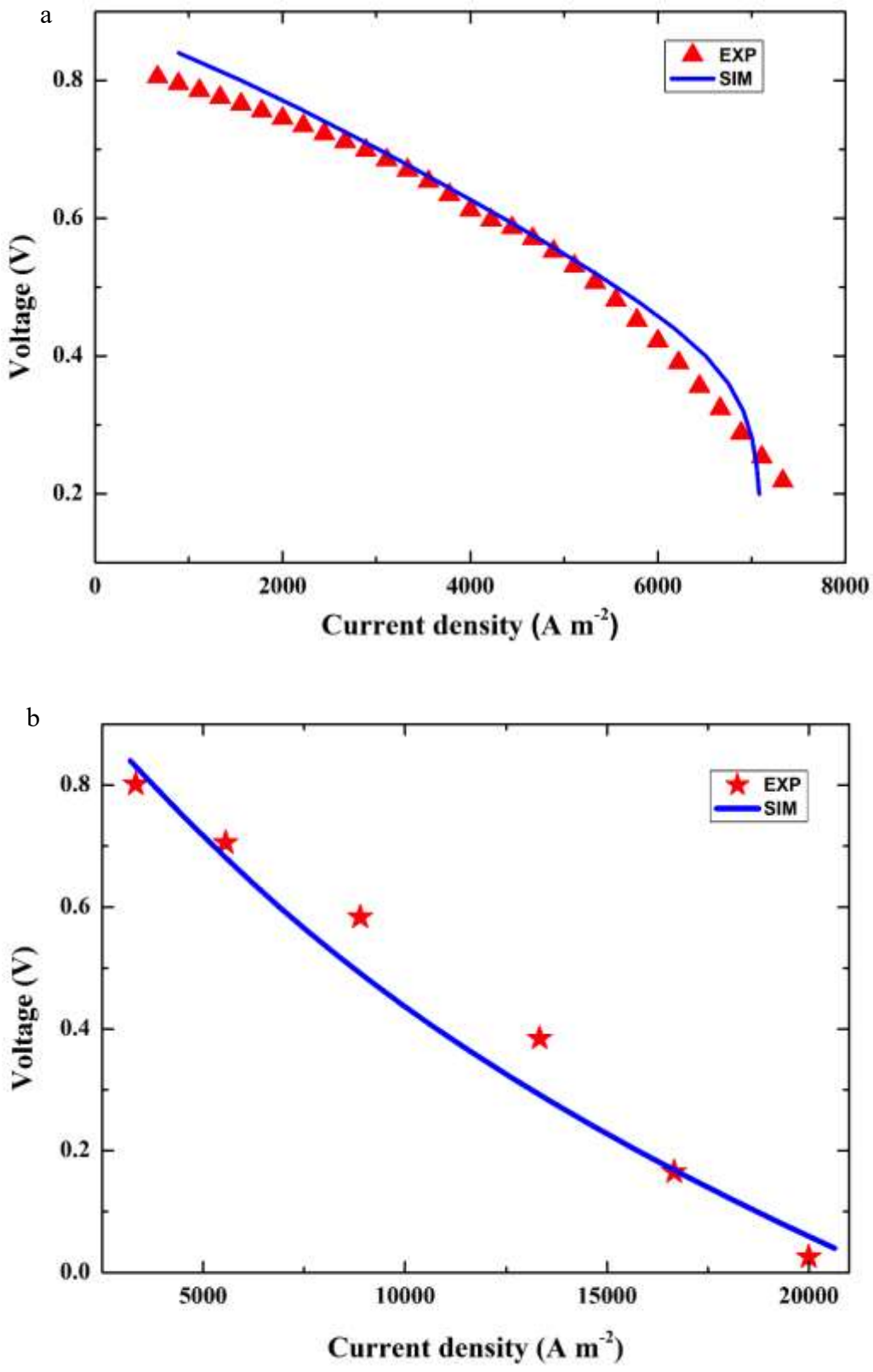

Fig.2 Model validation for DC-SOFCs using H_2O as agents without (a) and with (b) catalyst.

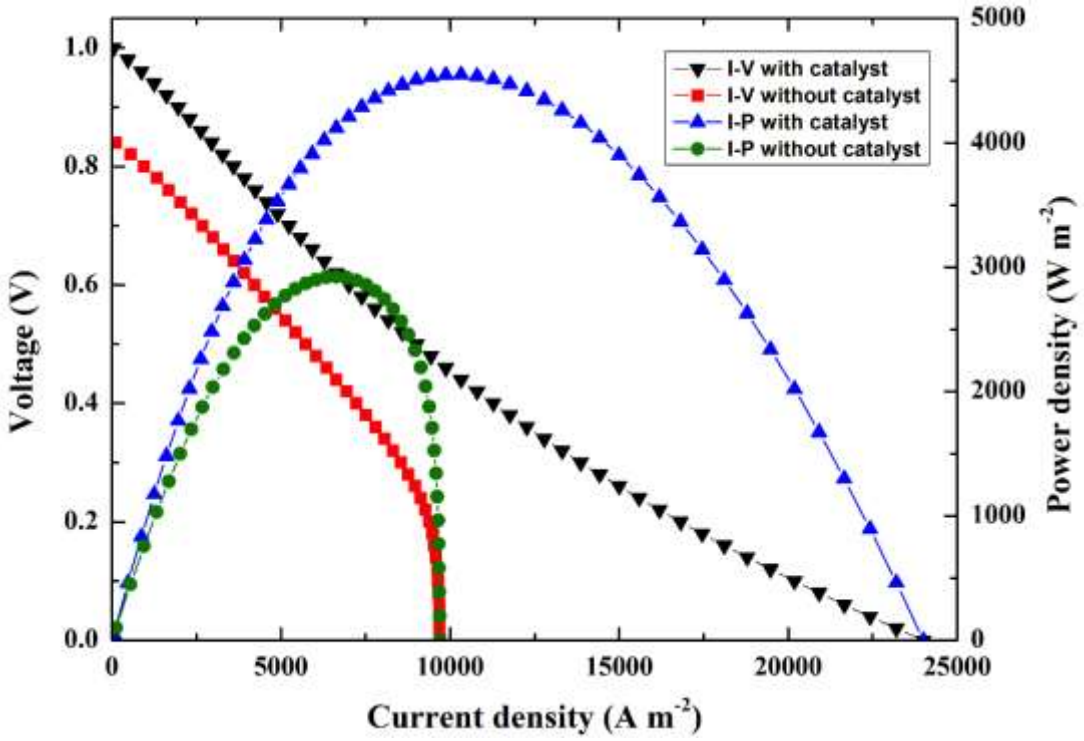

Fig. 3 The voltage-current density-power density relationships of DC-SOFCs using H_2O as agents with and without catalyst.

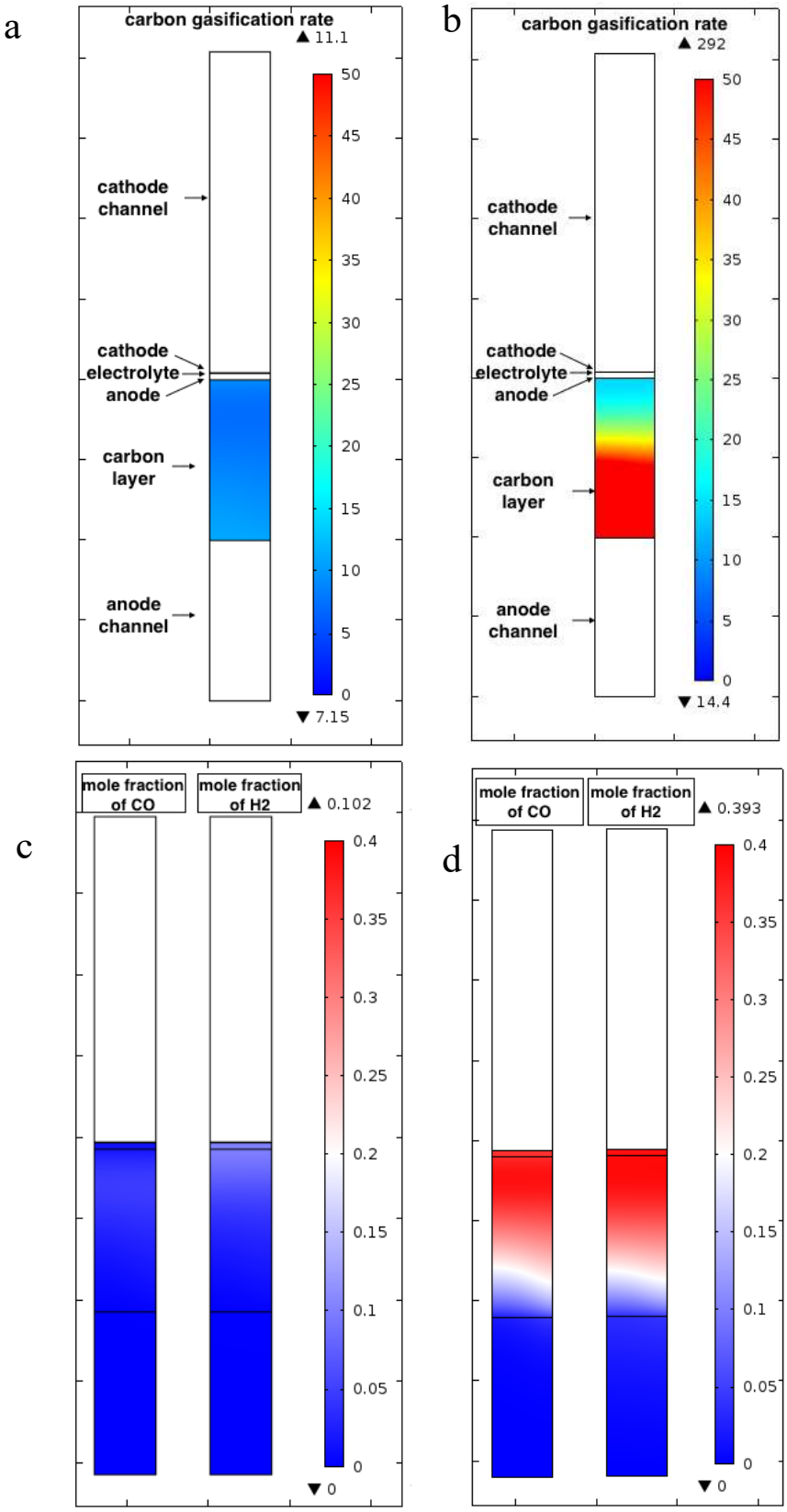

Fig. 4 The carbon gasification rate (mol m^{-3} s^{-1}) without (a) with (b) catalyst in carbon layer and mole fraction of fuel without (c) and with (d) catalyst in anode of DC-SOFCs at 0.8 V and 1123 K

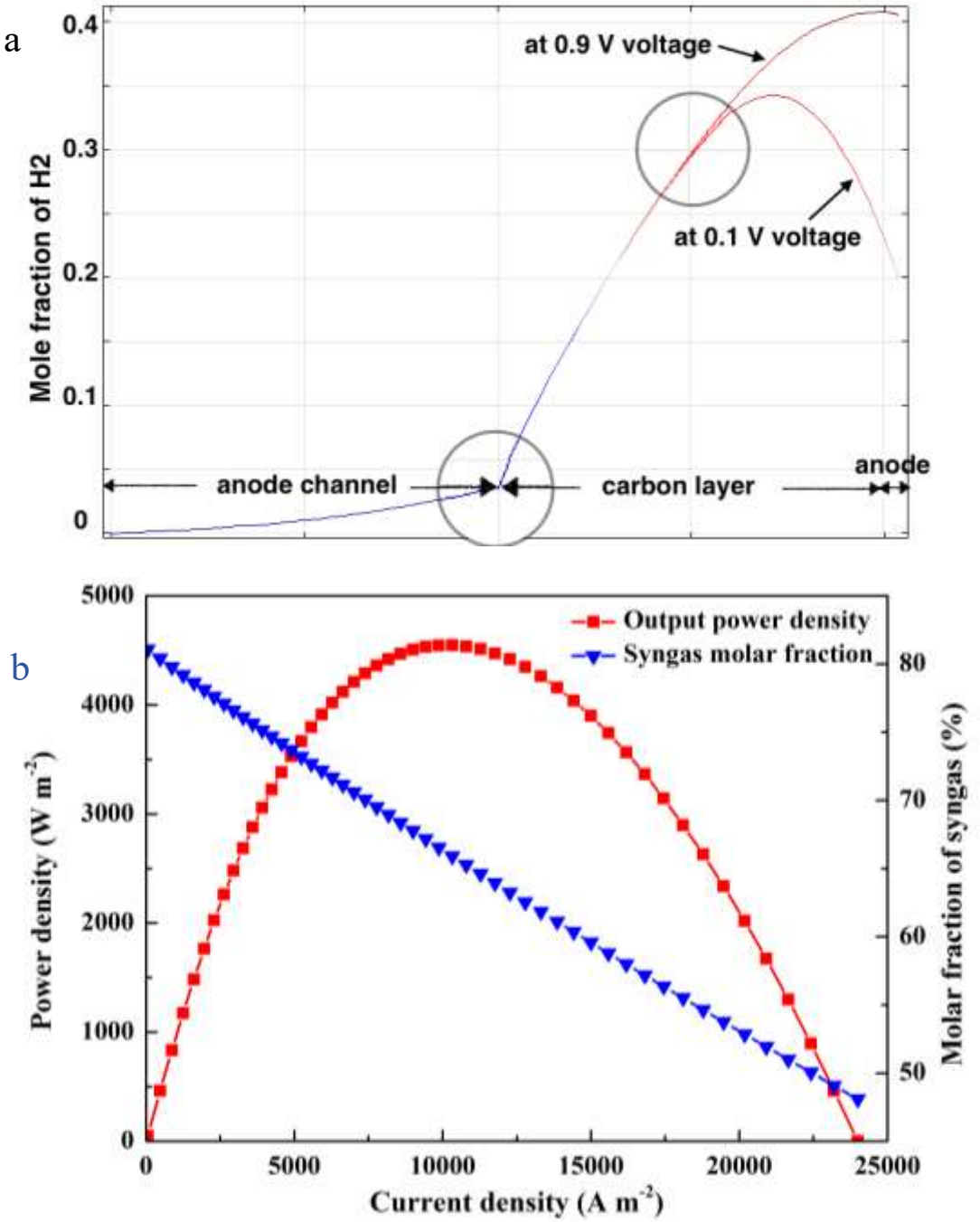

Fig. 5 (a)Distribution change of H_2 mole fraction in anode with catalytic gasification at 0.9 V and 0.1 V operating potentials and 1123K; (b) I-P characteristics and syngas molar fraction change at different operating current densities.

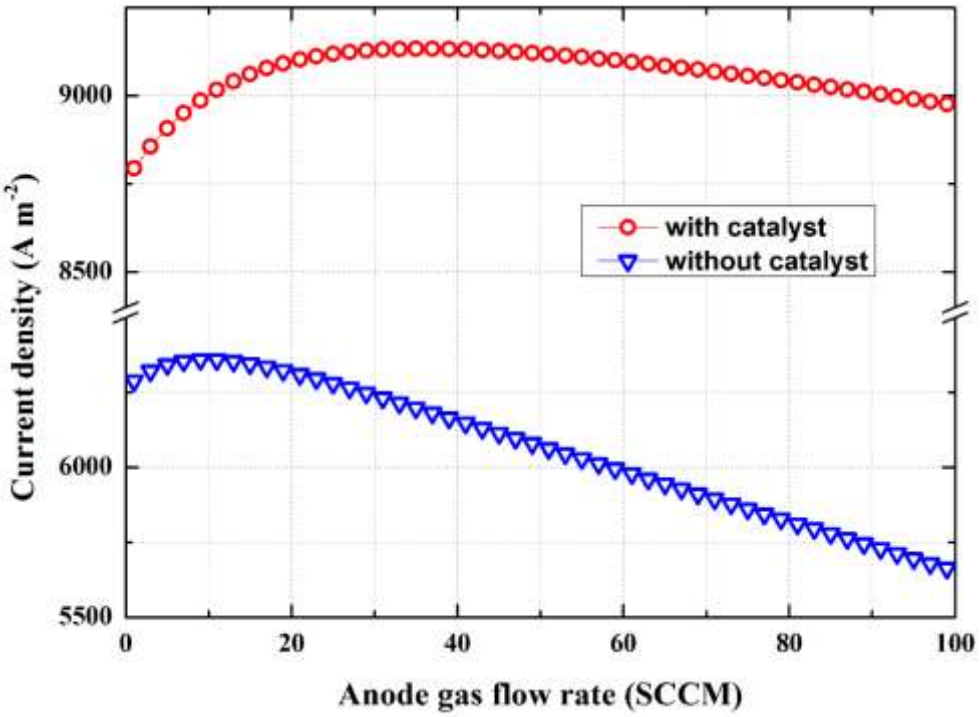

Fig. 6 The effect of anode inlet gas flow rate on current density of DC-SOFCs with H_2O as agents at 0.5 V and 1123 K

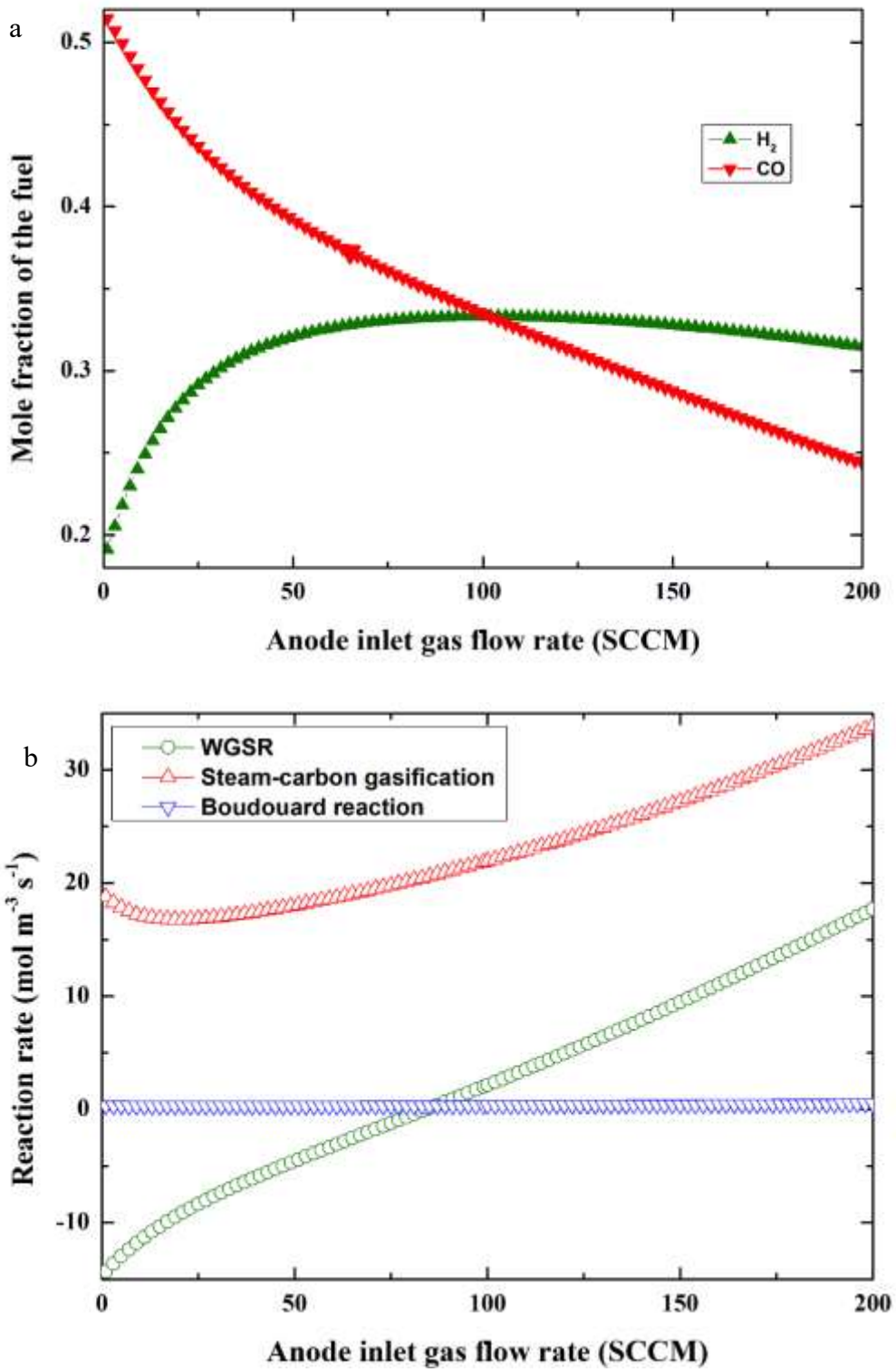

Fig. 7 The effect of anode inlet gas flow rate on fuel mole fraction (a) and chemical reaction rates (b) in anode surface of DC-SOFCs at 0.5 V and 1123 K

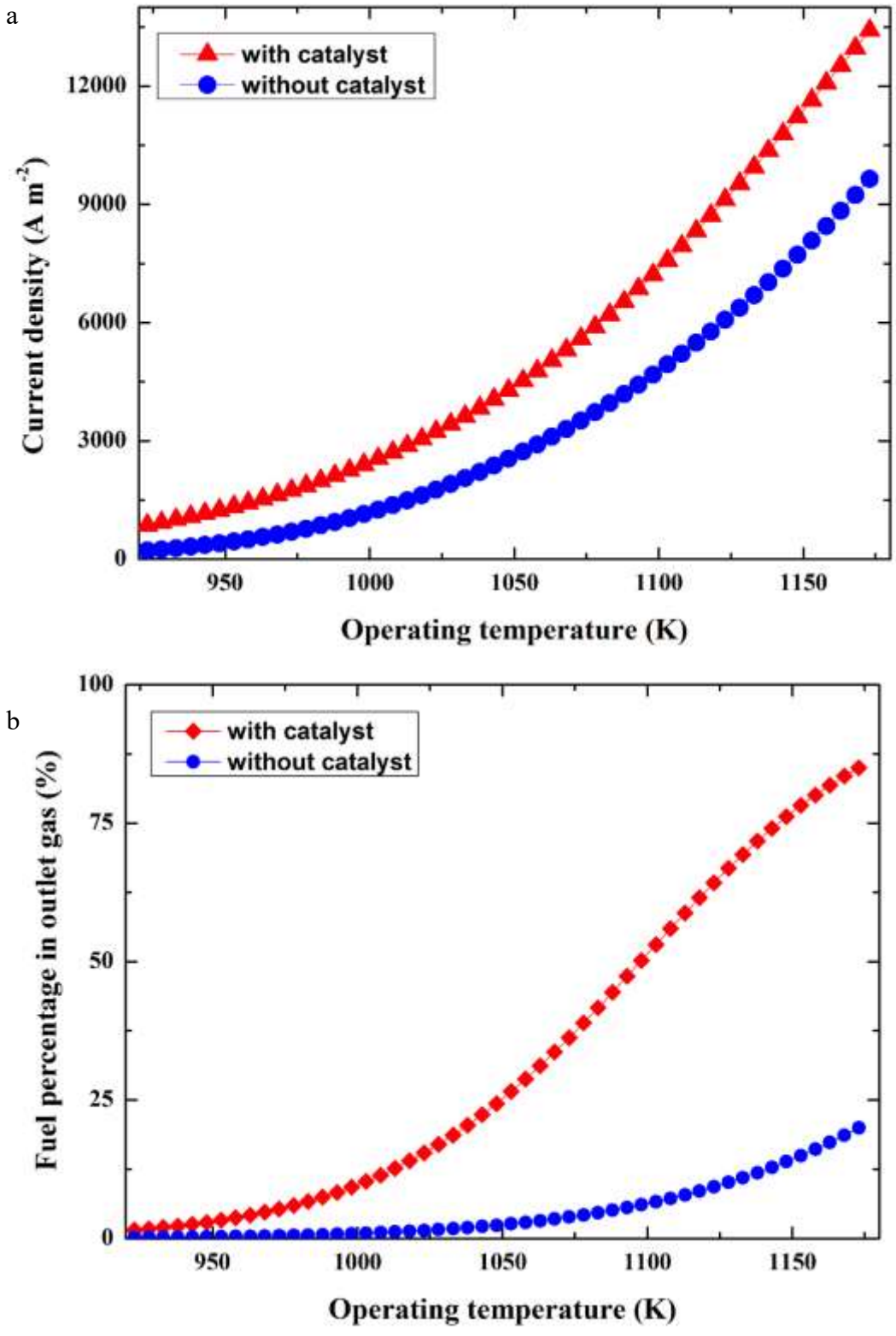

Fig.8 The effect of operating temperature on current density (a) and fuel percentage in outlet gas (b) of DC-SOFCs with H_2O as agents at 0.5 V operating potential